Topology Optimization of Wave Barriers for Mitigating Dynamic Compaction-Induced Vibrations Using a Coupled CMA-ES/Finite-Element Method

First author: Farzaneh Abedini

M. Sc. graduate in Geotechnical Engineering, School of Civil Engineering, University of Tehran, Tehran, Iran

PhD Candidate, Department of Civil Engineering, McGill University, Quebec H3A 0C3, Canada

Second author: Reza Rafiee-Dehkharghani (Corresponding Author); (rezarafiee@ut.ac.ir)

Assistant Professor, School of Civil Engineering, College of Engineering, University of Tehran, Tehran, Iran.

Third author: Karim Laknejadi

Assistant Professor, Islamic Azad University

1

Abstract

This paper aims to find optimal wave barriers for mitigating the ground-borne vibrations induced during dynamic compaction (DC). Within this context, two types of barriers are considered. The first type of barrier has a classic rectangular shape, and they are arranged in single, double, and quadruple configurations The second type involves a distributed grout barrier located within a designated area, characterized by varying grout densities. In this research, the finite element (FE) method is used to simulate the dynamic compaction problem, and soil nonlinearity is considered due to the development of large deformations around the tamping point in dynamic compaction. Covariance Matrix Adaptation Evolution Strategy (CMA/ES) serves as a robust optimization tool and is coupled to FE simulations using comprehensive Python scripts to find the optimal barrier configuration. The findings from the study reveal that the number of rectangular barriers does not necessarily increase mitigation capacity. Furthermore, the barriers' mitigation capacity (MC) depends on their filling material and filled percentage. Moreover, the investigation of distributed grout barriers reveals an interesting observation that the optimal configuration for the grout distribution tends to form an approximate W-shaped pattern.

1. Introduction

Vibration mitigation is a holistic concept, involving a wide array of methods aimed at effectively reducing vibrations. In some cases, base isolation can be implemented; but it is limited to active seismic zones considering the relatively high costs associated with implementation. Additionally, cost-effective yet efficient mitigation methods, such as wave barriers and ground improvement techniques, can be used (Jayawardana, Thambiratnam, Perera, & Chan, 2019). Open and in-filled trenches, piles, sheet piles, heavy mass technology, scrap tire isolation walls, and soil grouting can also be used for mitigating vibrations induced by heavy machinery and trains (Mahdavisefat et al., 2017; Saikia & Das, 2014). In general, wave barriers can be classified into two categories: stiff barriers and soft barriers, distinguished by their impedance mismatch with the soil. For instance, concrete-filled trenches are stiff barriers, while bentonite-filled trenches or gas cushions are soft barriers.

Svinkin (2004) categorized vibration consequences into three groups; structure vibrations, resonant structure response, and dynamic settlements. In the literature, the parameters of trench width, depth, and location are primarily studied. However, other factors, such as trench shape (Esmaeili et al., 2014; Yarmohammadi et al., 2018; Zakeri et al., 2014), buried depth (Feng et al., 2019; Moussa & El Naggar, 2020), and trench inclination angle (Cho, 2021; Herbut, 2020), are also investigated in the literature.

The conversion of Rayleigh waves to other types of waves, such as primary or secondary waves (P and S waves), is called mode conversion. The barrier functionality is evaluated based on the percentage of the waves spreading, reflecting, or refracting from the barrier. In open trenches, reflection plays the governing role; however, in the filled trenches, mode conversion is also of great importance. Installing trenches in the wave path causes discontinuity and lengthens the path. Thus, it may lead to a considerable decrease in wave energy. Moreover, Rayleigh wave amplitude diminishes along the depth. It is observed that vibrations decrease by 90% at a depth of 1.5 λ_R (Rayleigh wavelength). Barriers can be open or filled with different materials, such as water, concrete, and bentonite. Open trenches are the most effective ones since they can block wave transmission. However, researchers have always looked for new materials to fill the trenches.

3

For instance, some studies are performed to evaluate the efficiency of water, geofoam, concrete, bentonite, tire-derived aggregates (TDA), and tire chips (Alzawi, 2011; Ekanayake et al., 2014; Fathi Afshar et al., 2024; Moussa & El Naggar, 2020; Tandon et al., 2023). In case of instability, geofoam-filled trenches can be used instead of open trenches (Mahdavisefat et al., 2017). One of the novel methods of blocking vibrations is using metamaterials that control wave energy. Gao and Shi (2019) used barriers made of layered metamaterials, and frequency and time-domain analyses proved their satisfactory functionality. These barriers are called wave-guided barriers. Majumder and Venkatraman (2023) conducted a state-of-the-art review on vibration screening techniques using open and in-filled trenches.

Persson (2013) mentioned that when Rayleigh waves impinge on a filled barrier, five different scenarios happen for the incident wave; 1) Rayleigh wave that reflects from the trench; 2) Rayleigh wave that passes through the trench; 3) body wave that disseminates backward and deep in the soil; 4) body-wave that spreads in the domain; 5) body-wave that travels beneath the trench. Vibrations occurring in the locations after the trench are mainly due to types 2, 4, and 5.

Optimization has been used in geotechnical engineering for different usages, such as wave barriers (Jayawardana, Thambiratnam, Perera, et al., 2019; Sigmund et al., 2016), dynamic compaction (Bayat et al., 2023), and foundation design (Jelušič & Žlender, 2018; Juang & Wang, 2013; Sadeghi et al., 2021). Specifically, Yarmohammadi and Rafiee-Dehkharghani (2020), Rezaie et al. (2018), and Dolatshahi et al. (2020) applied topology optimization in studying wave barriers.

Analytical, numerical, or experimental methods can be utilized to study trenches' functionality. Numerical approaches, such as the boundary element method (BEM), finite element method (FEM), and finite difference method (FDM), are used since closed-form solutions are not always easy to achieve. Moreover, analytical methods are limited to simple boundary conditions and specific geometries. Additionally, experimental methods are often complex and expensive to implement. The promising results of previous numerical research validate the fidelity of numerical methods (Ahmad & Al-Hussaini, 1991; Bian et al., 2016; Mahdavisefat et al., 2017).

4

Either two-dimensional (2-D) or three-dimensional (3-D) models can be utilized in the analysis. Saikia and Das (2014) compared 2-D and 3-D models and concluded that 2-D models yield approximately 11-12% error. Moreover, research has demonstrated that 2-D simulations cannot fully capture geometric damping. It is beyond doubt that 3-D models are more accurate; however, their computational cost is significant (Norén-Cosgriff et al., 2019). Therefore, there is still a strong trend toward using 2-D simulations, particularly in optimization problems, where numerous numerical iterations are required.

This paper studies different governing parameters that affect the performance of wave barriers considering DC-induced vibrations. The affecting parameters are the trench's width and depth, the trench's location, and the filled percentage of the trench. Finding the most effective wave barrier is complex since all the previously mentioned affecting parameters are interdependent. Hence, the Covariance Matrix Adaptation Evolution Strategy (CMA-ES) is implemented to find the optimum topology of the wave barriers. The optimization algorithm is coupled with finite element (FE) simulations for finding the fitness function. Moreover, parametric studies and verifications ascertain the reliability of the results. Some researchers have studied the effectiveness of coupling optimization algorithms with FE simulation in complex optimal design problems (Rafiee-Dehkharghani et al., 2018). The studied barriers have two types: (1) rectangular barriers that are open, filled, or partially filled; (2) distributed grout with different densities that are scattered within a discretized domain using the topology optimization concept. The term "rectangular" refers to the barrier cross-section in the FE simulations. The rectangular barriers can be arranged in single, double, and quadrupole configurations. The studied problem and two proposed vibration mitigation approaches are detailed in the following sections. Further, modelling specifics, optimization methods, and results are presented in subsequent sections.

2. Problem definition

Dynamic compaction (DC) tamping generates surface vibrations due to the generation of Rayleigh waves. Two approaches are chosen to control the vibrations with wave barriers: (1) designing rectangular trenches and (2) distributing grout in the domain to find the optimal topology of the barrier.

5

In the first approach, one, two, or four (the determination of the maximum number of trenches is based on the limitations imposed by the width and distance within the domain) trenches can be installed in the disturbed zone. The efficiency of the trenches depends on various parameters, such as geometry, location, filling material properties of the barriers, and filled percentage. The primary objective is to trap these waves by installing wave barriers between the loading and receiving/observation points. It is not feasible to install the barriers in the close vicinity of the excitation and receiving points; thereby, a clear distance of L_R and L_T is considered as shown in Fig. 1. The domain that remains in between is called the optimization/disturbed zone. Moreover, a minimum distance of 0.5 m is maintained between trenches in case of multiple trenches for considering practical limitations. The general schematic of the DC problem studied in this paper is shown in Fig. 1, where w_b, d_b, and L stand for the trench's width, depth, and distance from the tamping point, respectively.

In the second approach, the grout is distributed in the design domain to find the best topology for the ideal wave barrier. Thereby, the domain is discretized into smaller cells (1×1 m), with grout distributed within these cells.

Due to the large solution domain and the interdependence of these parameters, conducting separate parametric studies to assess their influences is not feasible. As a result, it is required to use optimization algorithms such as CMA-ES to find the optimal configuration. The objective function of the optimization is minimizing the peak particle velocity (PPV) at the receiving point. The 2-D axisymmetric model and Mohr-Coulomb constitutive law are used in FE simulations of the problem. A similar constitutive law is used by Pan and Selby (2002), and it is observed that the Mohr-Coulomb model can successfully simulate the DC phenomenon. The Mohr-Coulomb model is a suitable option since it is not always easy to find the values of necessary parameters of other constitutive models (Mehdipour & Hamidi, 2017). In this vein, more complex constitutive models do not always outperform simpler ones, as they often present challenges in parameter calibration. The Mohr-Coulomb model is utilized in this research, considering that the focus

6

is on the optimization process. The schematic of the axisymmetric problem for approach 1 and 2 is depicted in Fig. 1

3. Numerical modelling and DC loading

Finite element (FE) numerical simulations are used for modelling the DC problem in this paper. To do so, ABAQUS commercial software is used to capture the transient dynamic loading nature of the tamping phenomenon. Soil is assumed to have a homogenous, isotropic, and elastoplastic medium. Material nonlinearity is considered as the DC-induced strains are large. The axisymmetric model is used in this study due to the symmetry of the problem and reducing the computational cost and the FE domain is selected to be large enough to prevent the wave reflections from the boundaries (Fig. 2). The model dimension is tailored based on the total loading duration to ensure that the waves reach the observation point, but do not reflect and affect the results. The observation point is located 17 m from the tamping point. The location of the observation point is chosen based on practical matters.

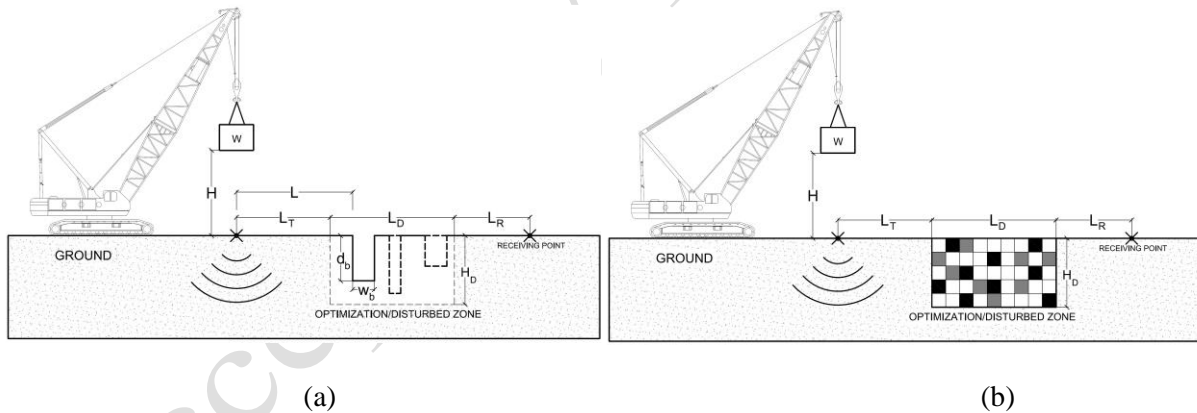(a)   (b)

Fig. 1. Schematic of the problem and two approaches for vibration mitigation; a) approach 1: single or multiple barriers, b) approach 2: material distribution or topology optimization.
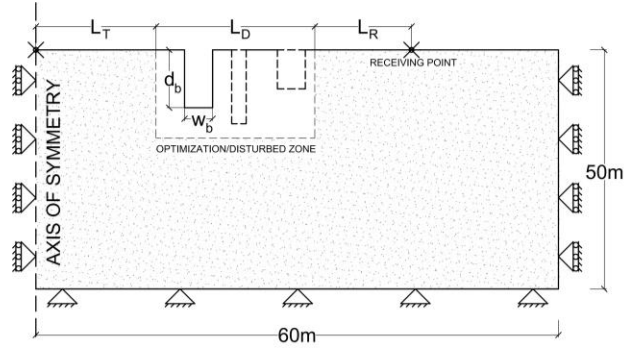
Fig. 2. Axisymmetric FE model.

3.1. Loading

The impact load induces surface displacements. Regarding propagation, Rayleigh waves are considered to be surface waves, meaning they travel on the top layers of the soil. They propagate outward from the source of the excitation, affecting a wide area of the surface.

Modelling Dynamic Compaction (DC) in detail is complex, involving numerous parameters that describe the interaction between the tamper and soil upon impact. Due to DC's cost-effectiveness as a ground improvement technique, these parameters are often not readily accessible. Moreover, incorporating all these intricacies into the model increases computational costs without necessarily improving accuracy. Therefore, it is required to use simplified methods for modelling DC loading. Within this context, Pan and Selby (2002) studied DC using ABAQUS models under two loading cases: 1. applying an approximate half-sine force-time profile on the ground; and 2. detailed tamper impact modelling. It was demonstrated that a half-sine loading graph simulates the tamping scenario well (Mayne & Jones Jr, 1983; Scott & Pearce, 1975). Fig. 3 shows the soil stress induced by a 10-ton rigid mass dropping from the height of 11.5 m (Abedini et al., 2022). To model the impact scenario, the velocity of the $\sqrt{2gh}$ (where g is the gravity acceleration and h is the dropping height) is applied to the tamper's reference point, and the force history profile is extracted at the tamping interface as shown in Fig. 3 considering the rigid contact between the soil and tamper. Furthermore, the PPV of the soil nodes at different locations from the tamping points is extracted for two types of loadings (half-sine load estimation and rigid impact modelling) and compared in Fig. 4. The results

8

in this figure show that the PPVs obtained using the simplified half-sine loading closely align with those from more detailed impact modelling; therefore, the DC loading is simulated by a half-sine profile. This is computationally very efficient as this paper focuses on optimizing the barriers.
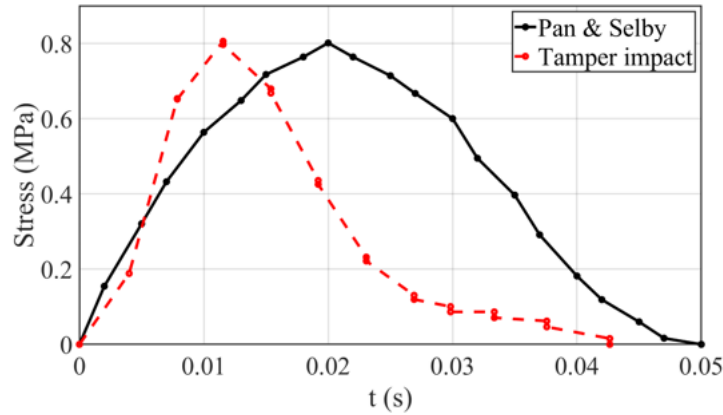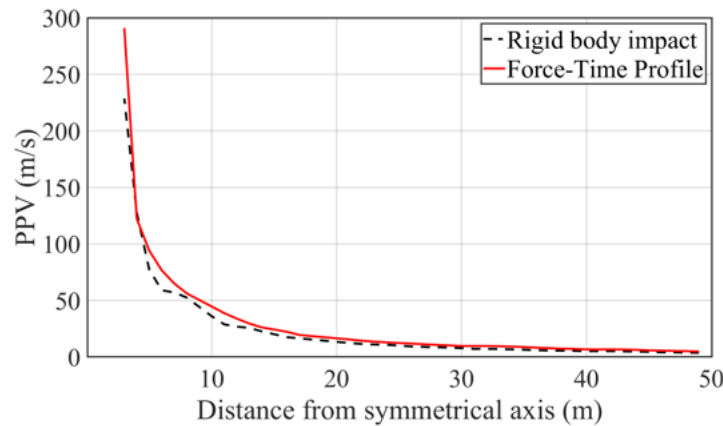

Fig. 3. Half-sine tamping loadings.

Fig. 4. Soil nodes PPVs at different distances.

3.2. FE mesh size and time step

Spatial and time discretization are very critical factors for accurate FE modelling. Using small elements increases the accuracy and the computational cost; hence, it is required to find an optimal mesh size using convergence analysis. Since the model is axisymmetric, CAX4R elements (4-node axisymmetric elements in the ABAQUS library) are used to mesh the model domain. Having approximately ten nodes per

9

wavelength is recommended, as this directly affects both time and computational costs (Norén-Cosgriff et al., 2019). In this study, the Rayleigh wave velocity of the soil and the loading frequency are 30 m/s and 10 Hz, respectively. Therefore, the maximum mesh size is $0.2 \times \frac{30}{10} = 0.6$m. Additionally, convergence analyses are conducted to ensure accuracy, with the final maximum size selected as 0.5 m.

The dynamic analyses are performed using ABAQUS/Explicit Solver. The time increments (Δt) are selected based on the maximum element size and wave speed in the soil. This is automatically selected in the explicit solver. For more detailed information on this topic, it is recommended to refer to the ABAQUS manual (Abaqus, 2014) which provides comprehensive guidance and instructions.

4. FE model verification

One of the main challenges in verifying numerical models is the limited availability of comprehensive data. Many field studies, especially older ones, do not provide sufficient data for building and calibrating numerical models. To verify the results, a model is constructed using sandy soil characterized by the properties listed in Table 1. Two different tampers with masses of 10 and 25 tones are dropped separately from a height of 10 m and 20 m, respectively. Figure 5 exhibits a perfect match between the results obtained from the finite element (FE) models and the field measurements conducted by Lukas (1986). This correspondence validates the accuracy and reliability of the FE models in capturing the real-world behaviour of the DC. In Fig. 5, m and H denote the tamper mass and drop height, respectively.
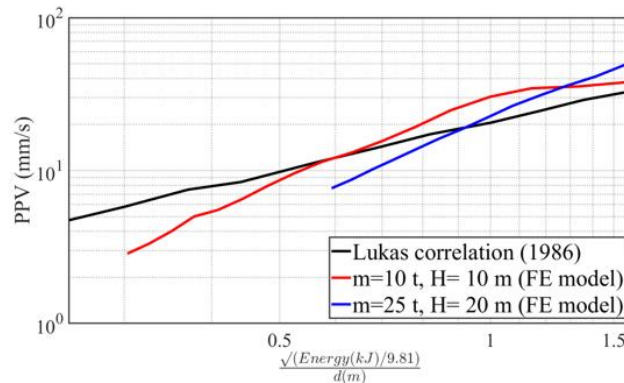

Fig. 5. FE model verification

Table 1. Sandy soil properties for verification

ρ	ν	φ	E
$1600\ (\dfrac{\text{Kg}}{\text{m}^3})$	0.25	30 degrees	25 MPa

5. Material properties of the ground and barriers

The soil properties are elaborated in Table 2, where V_s and V_R represent the shear wave velocity ($V_s = \sqrt{\dfrac{E}{2\rho(1+\nu)}}$) and Rayleigh wave velocity ($V_R = V_s \times \dfrac{(0.862+1.14\nu)}{(1+\nu)}$), respectively. Damping is a critical issue in dynamic analysis. Rayleigh damping is applied in the model with the coefficients of $\eta_1 = 0$ and, $\eta_2 = 0.01$. Where η_1 and η_2 are mass damping coefficient and stiffness damping coefficient, respectively. (1) shows the Rayleigh damping formula where ω is the circular frequency, and α and β are Rayleigh damping coefficients (Chopra, 2007).

$$\xi = \frac{1}{2\omega}\alpha + \frac{\omega}{2}\beta \tag{1}$$

Filling material is one of the governing factors in trenches. In other words, the impedance mismatch ratio (IR) between the soil and the filling material of the trench affects waves' transmission. Impedance mismatch between the soil and the filling material significantly affects the efficiency of the wave barriers. A high IR shows a significant difference in impedance between the materials which leads to reflections of waves at the interface. These reflections can result in wave energy being directed back into the soil or spread through the barrier. IR is defined in Eq. (2) and is zero for the open trench. The mechanical properties of the filling materials (concrete and soil-bentonite mixture (SBM)) used in this paper are detailed in Table *3*.

Table 2. Ground properties

Elastic modulus (E)	Friction angle (φ)	Cohesion (C)	Poisson's ratio (ν)	Density (ρ)	V_s	V_R
5 MPa	25 degrees	5 KPa	0.35	1800 kg/m^3	32 m/s	30 m/s

$$IR = \frac{\rho \times V_{s\,\text{filling material}}}{\rho \times V_{s\,\text{soil}}} \tag{2}$$

Table 3. Filling material properties

Filling material	$\rho \left(\frac{Kg}{m^3}\right)$	E (MPa)	ν	$V_s \left(\frac{m}{s}\right)$	IR
Concrete	2400	20000	0.15	1903	79
SBM	1200	3.13	0.45	30	0.63

6. Optimization method

Topology optimization is one of the important methods of optimization. By employing topology optimization techniques, the barriers are engineered to disrupt and attenuate the transmission of waves induced by dynamic compaction. Rayleigh waves have the highest energy and are the most destructive ones, thereby, the main attention and discussions are on Rayleigh waves. Different objective functions, such as displacement, velocity, and compliance, can be defined based on the problem's purpose. Minimizing the vertical PPV at the receiving point is the objective function of the optimization in the current study. PPV is measured by obtaining the velocity record from ABAQUS and finding the maximum of the absolute values. In this paper, topology optimization of barriers is studied using CMA-ES. Meta-heuristic algorithms, such as CMA-ES, treat the problem as a black box, providing a specific response for any given inputs; hence,

12

they can solve a wide range of optimization problems. This strategy is based on the normal distribution and uses covariance matrix (C), population size (λ), mean (m), and step size (σ). Covariance shows the variables' dependency and controls the shape of the distribution ellipsoid. The mean vector represents the favourite solution, and the step size controls step length. These parameters are continually updated in each iteration based on the outcomes of previous steps. Many references on CMA-ES optimization are available in the literature, among which the interested readers are referred to (Hansen, 2019; Hansen & Auger, 2014). CMA-ES is a robust adaptive meta-heuristic strategy for optimizing continuous variables. Its speed and computational cost are satisfactory. Therefore, it is a suitable optimization method for the current problem. For instance, CMA-ES has outranked 31 other optimization methods in one research of Black-Box optimizations (Hansen et al., 2010).

At each population or optimization step, the geometry of the ABAQUS FE model changes and needs to be updated. Applying these changes in each population using the graphical user interface of ABAQUS is a time-consuming and fairly impossible process. Therefore, the connection between the optimization algorithm and FE models should be automated; in other words, they need to be coupled. Comprehensive Python codes are developed to couple the optimization algorithm with FE models. These codes create new FE models based on different parameters defined within the optimization process. The following steps are performed in the Python scripts created for coupled CMA-ES/FE procedure:

1. Creating different parts of the FE model, allocating different material properties and sections based on the optimization variables developed in the optimization process; 2. applying loads and boundary conditions to the model; 3. meshing the model with appropriate mesh size; 4. simulating the FE model using dynamic explicit analysis; 5. exporting the FE model outputs to a file to be used in the updating process of the objective function.

This process continues until the termination criterion is satisfied (here set to 10^{-2}, setting 10^{-2} as the termination criterion means optimization stops when the range between the best objective function values of recent and past generations is less than 10^{-2}. The selection of the termination limit depends on the

13

problem.). Multiprocessing is utilized in certain cases due to the high computational cost (multiprocessing with five cores in single trenches, and two cores in dual and quadruple trenches).

6.1. Optimization of the rectangular trenches

Optimization variables are width (w_b), depth (d_b) and trench's distance from the tamping point for the open, filled, and partially-filled rectangular trenches (L). In addition to the stated variables, a filled percentage (FP) is considered as the fourth variable in the partially-filled trenches. Width varies between 1 to 2 m, depth ranges between 1 to 7 m, location can have values between 2 to 12 m, and filled percentage ranges between 0 to 100 percent. The optimization constraint is applied to the total excavation volume and is set to be $10\frac{m^3}{m}$. This constraint ensures that the excavation volume remains within the specified limit. It is assumed that an excavation volume of more than $10\frac{m^3}{m}$ is not economically and operationally suitable.

6.2. Material distribution in the domain

Topology optimization searches for novel designs within a specified domain adhering to the specific constraint of an excavation volume of $10\frac{m^3}{m}$ in this study. In this case, the optimization zone is discretized into 1×1m cells (77 grids) within a 7m $\times$ 11m domain, as illustrated in Fig. 1 (b). The selection of cell size should achieve a balance between accuracy and computational efficiency, ensuring robust results for the problem. Optimization variables are densities assigned to each cell within the optimization zone. The optimization algorithm generates 77 different densities (optimization variables), each ranging from 0 to 1. A density of 0 indicates the cell is not grouted (pure soil), while 1 signifies a fully grouted cell. While intermediate values between 0 and 1 are generated during the optimization process, the optimal design ideally consists only of 0s and 1s. A penalization factor (P) is defined based on Eq. (3), where k stands for the iteration step to decrease intermediate values. P increases according to generation increase, reaching a value of 5 at maximum (Groenwold & Etman, 2010; Seitz & Grabe, 2016). Soil properties in each cell are calculated by interpolating between the soil and grout properties based on Eq. (4) showing interpolation of

14

elastic modulus for each grid (E_{grid}) using density (ρ) and penalization factor (P). This interpolation can also be used for other material properties (Seitz & Grabe, 2016).

$$P = \begin{cases} 1 & , \quad k < 10 \\ \min(5, 1.021^{k-10}) & , \quad k \geq 10 \end{cases} \tag{3}$$

$$E_{grid} = E_{soil} + \rho^p \times (E_{grout} - E_{soil}) \tag{4}$$

Grout properties are indicated in Table 4. Grout properties are calculated based on the case studies reported in Toraldo et al. (2018). The grout density is chosen the same as that of soil as recommended by Croce et al. (2014) . Young's elasticity modulus is calculated based on Eq. (5), where C stands for cohesion and β is a dimensionless coefficient which depends on soil type. Based on case studies reported in Toraldo et al. (2018), β ranges between 330 to 830 for silty sand. For this study, a value of 400 has been selected, and α is subsequently calculated using Eq. (6). Cohesion and friction angle values are chosen based on the study by Toraldo et al. (2018).

$$E = \frac{C}{\alpha} \times \beta \tag{5}$$

$$\alpha = \frac{1}{2\tan(\frac{\pi}{4} + \frac{\varphi}{2})} \tag{6}$$

Table 4. Grout properties

Elastic modulus (E)	Friction angle (φ)	Cohesion (C)	Density (ρ)
4 GPa	26 degrees	3.2 MPa	1800 kg/m^3

7. Results and discussion

This section discusses optimization results. Each optimization process is repeated at least twice to verify its accuracy and avoid local optima. The primary focus of using wave barriers is to attenuate vertical vibrations, particularly in cases where the ground loading is vertical, such as with DC loads in this paper. Attenuation is achieved through spreading, reflecting, or refracting waves from the barrier. Therefore, all simulations,

15

results, and suggestions provided in this section are related to the vertical direction. These results cannot be extrapolated to the horizontal vibrations as their mitigation pattern is entirely different from the vertical vibrations.

Results of two different approaches are presented separately in the following subsections. PPV is 21 mm/s at the receiving point without any trenches or grouting (i.e., pure soil). Mitigation capacity (MC) is defined by Eq. (7) to quantify the functionality of trenches, where design stands for the disturbed soil, and pure soil indicates the soil without any trench or grouting. The higher the MC, the more the trench functionality. MC is used to compare the trenches functionality in the subsequent sections.

$$MC = \frac{\text{Objective function}_{\text{design}} - \text{Objective function}_{\text{pure soil}}}{\text{Objective function}_{\text{pure soil}}} \times 100 \tag{7}$$

7.1. Rectangular trenches

Rectangular trenches have been examined in three distinct scenarios: single, dual, and quadruple trenches. The outcomes of each case are detailed in the following sections.

7.1.1. Single trench system

Optimization results are reported in Table 5 and

Table 6, in which L represents the distance between the loading and the trench, w_b and d_b stand for the trench width and depth, respectively. Installing trenches in the wave path causes discontinuity and lengthens the path. As results reveal (Table 5,

Table 6), open trenches have been found to be more effective compared to in-filled trenches due to the absence of energy transfer through them. Fig. 6 (a) to 6 (c) illustrates various trench configurations.

Partially filled trenches with concrete have shown effectiveness. Partially concrete-filled trenches with a 10% filled percentage (FP) have been found to offer the highest MC, which is 48.5% (Fig. 6 (c) and

16

Table 6). However, SBM- filled trenches are not suitable and yield results similar to open trenches (Table

5 and

Table 6).

Table 5. Optimized variables of open and filled trenches.

Material	Impedance Ratio	Optimized Variables				
		w_b(m)	d_b(m)	L (m)	PPV (mm/s)	MC (%)
Open	0	1.2	7.0	2.0	11.4	46.0
SBM	0.63	2.0	2.8	7.0	18.8	10.3
Concrete	79.0	1.4	7.0	8.7	20.0	4.9

Table 6. Optimized variables of partially-filled trenches.

Material	Impedance Ratio	Optimized Variables					
		w_b(m)	d_b(m)	L (m)	FP (%)	PPV (mm/s)	MC (%)
SBM	0.63	1.2	7	2.1	0	0	45.2
Concrete	79.0	1.3	7	6.3	10	10	48.5

Table 5 and

Table 6 show that deep active trenches are the most effective open trenches. The optimized depth reaches

the maximum allowable value in the optimization procedure, implying the close relationship between the

trench depth and vibration mitigation. Table 5 indicates that open trenches can mitigate the vibrations by

up to 46%, the field results reported by Fathi Afshar et al. (2024) showed that the open trenches can have
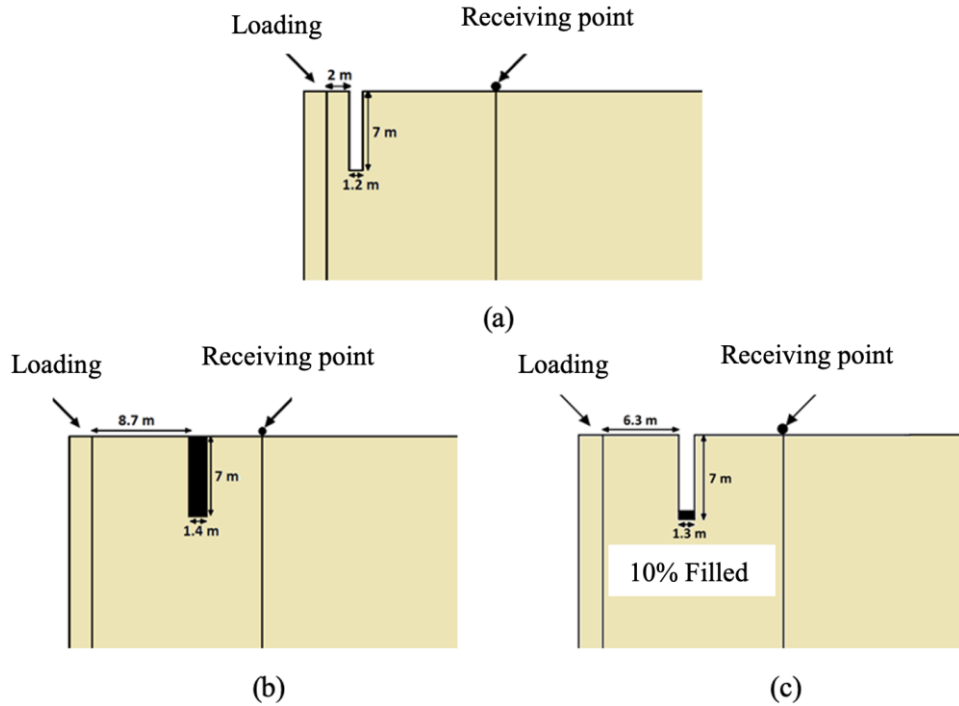
an effectiveness of 50%.

17

Fig. 6. Optimized configurations of single trench systems; a) Open, b) Concrete-filled, c) Partially concrete-filled

7.1.2. Dual system trench

The performance of open trenches surpasses that of other single trench systems. As a result, the current section focuses only on the study of open dual trenches. In this section, a similar constraint is defined over the volume of excavation ($10 \frac{m^3}{m}$) to make the results comparable with those for the single trenches. Table 7 elaborates on dual trenches system optimization results. Open dual trenches have similar constraints in width, depth, and distance as single trenches. In addition to the previously mentioned constraints, it is advisable to keep a minimum distance of 0.5 meters between each trench to address practical concerns.

The optimized layout of open dual trenches decreases the PPV value to 10.7 mm/s. Its performance is improved by 0.5% and 3% compared to partially concrete-filled and open single trenches in the previous section. As observed in Fig. 7, these trenches are relatively far from each other. The spatial separation suggests that trenches do not work together or have a significant influence on each other. It can be concluded that doubling the number of trenches does not significantly affect MC value.

Table 7. Optimized variables in dual trenches system

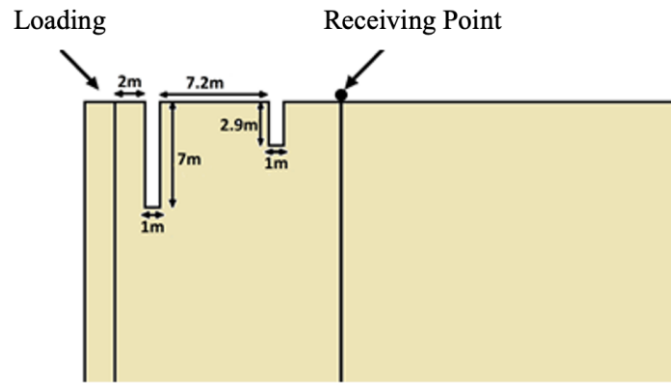| Trench number	Optimized variables				
	w_b (m)	d_b (m)	L (m)	PPV (mm/s)	MC (%)
Trench 1	1	7	2	10.7	49
Trench 2	1	2.9	10.2		

Fig. 7. Optimized variables of dual trenches.

7.1.3. Quadruple trenches system

In this section, four trenches are installed in the disturbed zone while keeping the total volume of excavation equal to the constraint in previous sections (i.e.,10 $\frac{m^3}{m}$). Table 8 shows optimized variables of the quadruple trenches system. The minimum depth of the trenches is assumed to be 0.1 m to study whether the increasing number of trenches is effective. In the optimization process, if trenches with very small depths are generated, it can be concluded that those trenches are not functional or effective, and it is better to remove them. As shown in Fig. 8, two middle trenches have the smallest possible depth of 0.1 m. This indicates that increasing the number of trenches does not necessarily increase MC value. By comparing the results in Fig. 7 with those in Fig. 8, it can be observed that the optimal quadruple trenches are very similar to the optimized dual trenches. This observation verifies the fidelity of the optimization procedure and underscores that increasing the number of trenches might not necessarily be effective. It suggests that

19

blindly adding more trenches does not guarantee improved results and that careful consideration should be given to the design and placement of trenches.

Table 8. Optimized variables in the quadruple-trenches system

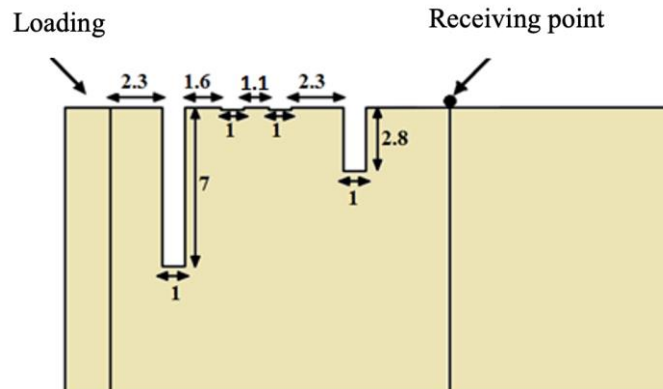| Trench number	Optimized variables				
	w_b(m)	d_b(m)	L (m)	PPV (mm/s)	MC (%)
Trench 1	1	7	2.3		
Trench 2	1	0.1	4.9	10.77	49
Trench 3	1	0.1	7		
Trench 4	1	2.8	10.3		

Fig. 8. Optimized variables of the quadruple-trenches system (values are in meters. This is not indicated in the figure due to space constraints).

7.1.4. Changing the objective function

In this study, the objective function aims to minimize the vertical PPV at the receiving point. Vertical PPV has been used as the major parameter for measuring vibration in previous research; however, in some papers, acceleration or displacement are considered alternative parameters for measuring vibrations. The choice of the vibration measuring parameter depends on the specific objectives of the study and the available data. To investigate the impact of the objective function definition, two additional optimizations

are performed, assessing the objective function using acceleration and displacement values. These simulations are performed for single open trenches and the results are presented in Table 9.

It is observed that changing the objective function from velocity to acceleration does not make a significant difference in the optimized variables; however, the related MC increases considerably from 46% to 75% (Table 9). On the other hand, the objective function defined based on the displacement results in a different optimized location for the trench. However, it still emphasizes the necessity of using a deep active trench. Based on observations, it has been noticed that the variation range of acceleration is more pronounced compared to displacement. Acceleration tends to exhibit more tangible variations in response to changes in each studied variable. On the other hand, displacement shows minimal variation and is not significantly sensitive to variations in optimization variables.

Table 9. Optimization results for different objective functions.

Objective function	Optimized variables			
	w_b (m)	d_b (m)	L (m)	MC (%)
Peak particle velocity	1.2	7	2	46
Peak particle acceleration	1.2	7	2.1	75
Peak particle displacement	1.4	7	5.7	26

7.2. Material distribution in the domain

In this section, a more complex optimization problem is solved using the CMA-ES/FE approach to optimally distribute the grout within the design domain. As previously mentioned, the optimization procedure inevitably generates intermediate densities (between 0 and 1); however, the penalization factor is applied to the density values to avoid intermediate densities as much as possible. Different densities are allocated to each cell to use these values in practice. Assigning different properties in practice can be achieved by modifying the ratio of materials in the mixture or changing the jet grouting process intensity.

Fig. 9 illustrates the designed wave barrier with grout distribution, and the presented distribution results in 35% mitigation capacity and a PPV of 13.6 mm/s.

As illustrated in Fig. 9, the grout is mostly concentrated in the lower parts of the disturbed zone due to the low-frequency range of the DC loading. Since the frequency range is low, the Rayleigh wave's penetration depth is deeper, resulting in denser distribution at the bottom of the zone. Moreover, grout is mostly located near the excitation source and the receiving point. Density values are larger near the tamping point and create a deep and active pattern similar to the results observed with rectangular trenches. The total material distribution creates an approximate W-shaped design. The W-shaped design traps the wave within the domain and makes waves' transmission to the receiving point harder. As a result, the waves that reach the receiving point are mitigated in intensity. The interpretation of W-shaped grout is that the concentration of grout near the excitation source minimizes the initial influence on the surrounding structures and putting the grout in the proximity of the receiving point ensures blocking the propagated waves before they reach the critical point.

0.21	0	0	0	0	0.29	0.14	0	0.04	0.37	0.15
0	0.25	0.53	0	0	0	0	0	0	0	0.14
0.12	0.01	0.03	0	0.02	0.00	0.31	0	0	0	0.01
0.01	0.95	0.04	0	0.19	0.13	0	0.01	0	0	0.47
0	0.86	0.08	0	0	0	0.24	0	0	0.21	0
0	0.16	0.66	0	0	0.95	0	0.05	0.33	0.24	0.01
0.47	0	0	0	0.15	0.07	0	0.44	0.35	0.08	0.03

Fig. 9. Each cell's density in the disturbed zone grid.

8. Verification of optimization results

A comprehensive parametric study is conducted in this section to examine the accuracy of the optimization results. Approximately 3500 models are built to analyze the single trench case, and nearly 6200 models are built to investigate the behaviour of dual trench system. The studied parameters include the width, depth, distance from the tamping point, and filled percentage. Width ranges between 1 to 2 m, depth varies between

1 to 7 m, distance from the tamping point varies between 2 to 12 m, and the filled percentage has values ranging between 0 to 100 percent. For brevity, this section includes only a selected number of graphs (Fig. 10 to Fig. 13) for reference.

Fig. 10 (a) illustrates the parametric study results in an open trench. A 1 m wide and 7 m deep trench located at 4 m from the centerline of the model has the minimum PPV, and it fully aligns with the optimization results presented in Table 5 (the distance values in Table 5. Optimized variables of open and filled trenches. Fig. 10 (b) depicts the results of the parametric study in the concrete-filled trench. The minimum PPV occurs when a 1 m wide and 7 m deep trench is located at 10 m or 12 m from the centerline, to which the optimization suggests a very close result (Table 5). Fig. 10 (c) indicates the parametric studies in an SBM-filled trench. A 1 m wide and 2 m deep trench located 4 m from the centerline generates the minimum PPV. The optimization result (Table 5) leads to a 2.8 m deep trench located at 9 m from the centerline. The optimization result differs from the parametric study, but it can be seen that the variation range is not wide, and the PPV of trenches located at 6, 8, 10, and 12 m from the centerline are marginally higher for a 2 m deep trench. Also, the second minimum happens when a 3m deep trench is located 10m from the centerline.

As depicted in Fig. 10, no specific trend is gleaned in the graphs, emphasizing the need to optimize problems as indefinite and unpredictable as the current study. Fig. 10 presents the amplifications observed in the study. It is noteworthy that the amplification phenomenon in impact loadings has been documented in only a limited number of studies. Amplification in vibrations induced by a forge hammer noted by Svinkin (2004), and the occurrence of amplification in open trenches in a pile-driving study reported by Jayawardana et al. (2018), further support the observation of amplification in specific scenarios. A study by Kermani et al. (2024) also found that increasing the trench depth does not follow a consistent trend, suggesting the presence of an optimal depth range for these barriers.

Indeed, the observed trend of amplification in impact loadings can be attributed to the presence of geometrical irregularities introduced during the installation of trenches. These geometrical irregularities

23

can cause wave reflections, diffractions, and scattering. As a result, certain frequencies or points may experience amplification of vibrations.
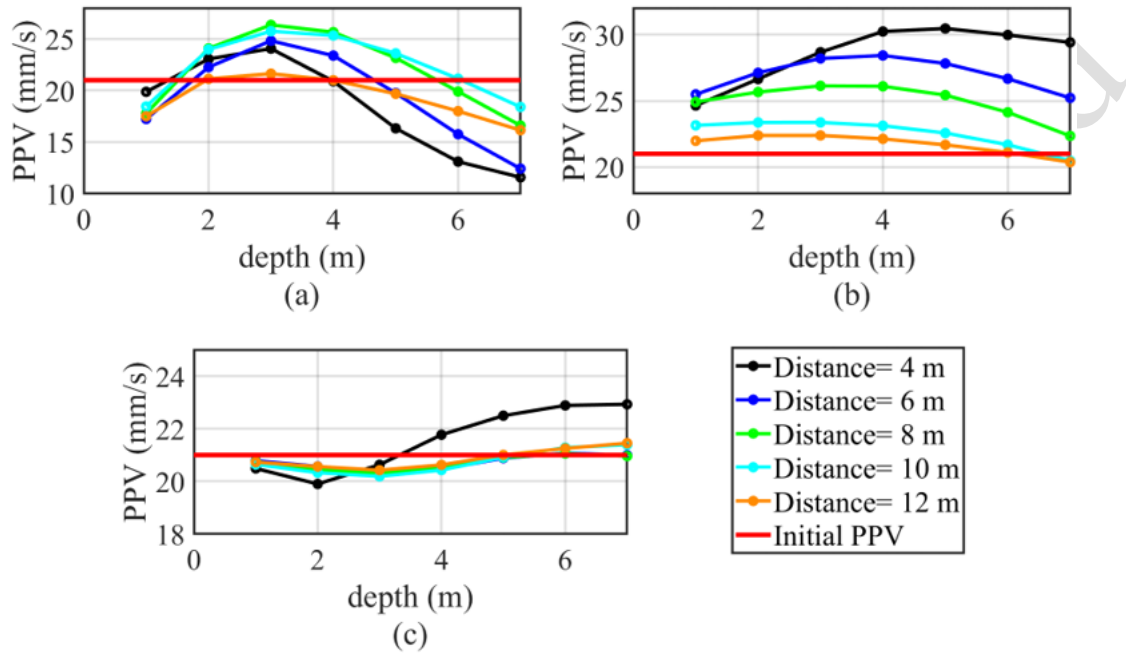

Fig. 10. Parametric study for single trench: a) Open trench, b) Concrete-filled trench, c) SBM-filled trench.

Moreover, Fig. 11 shows that partially SBM-filled trenches perform the best when empty (air-filled), especially with a depth of 7 m located at 4 m from the centerline. Fig. 11 confirms the optimization procedure's accuracy. Fig. 12 highlights the results in partially concrete-filled trenches. As observed, the minimum PPV is related to a trench that is 7 meters deep and 10% filled located at 8 m from the centerline. The optimization results report the same data, which indicates consistency and accuracy.
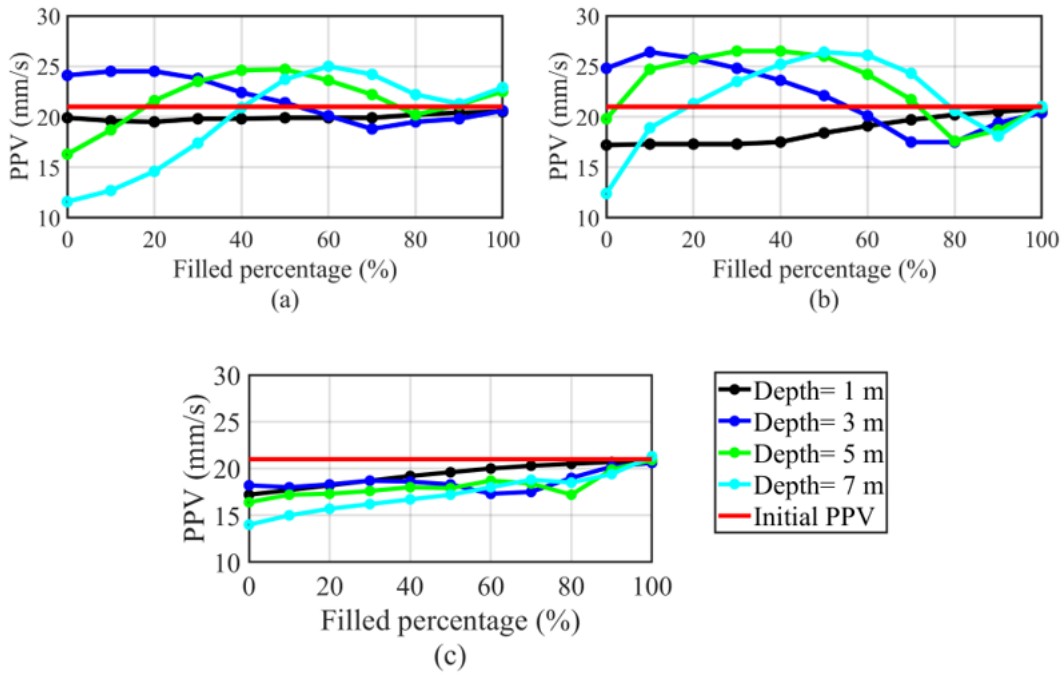
Fig. 11. Parametric study for partially SBM-filled single trenches located at a) 4 m, b) 8 m, c) 13 m.
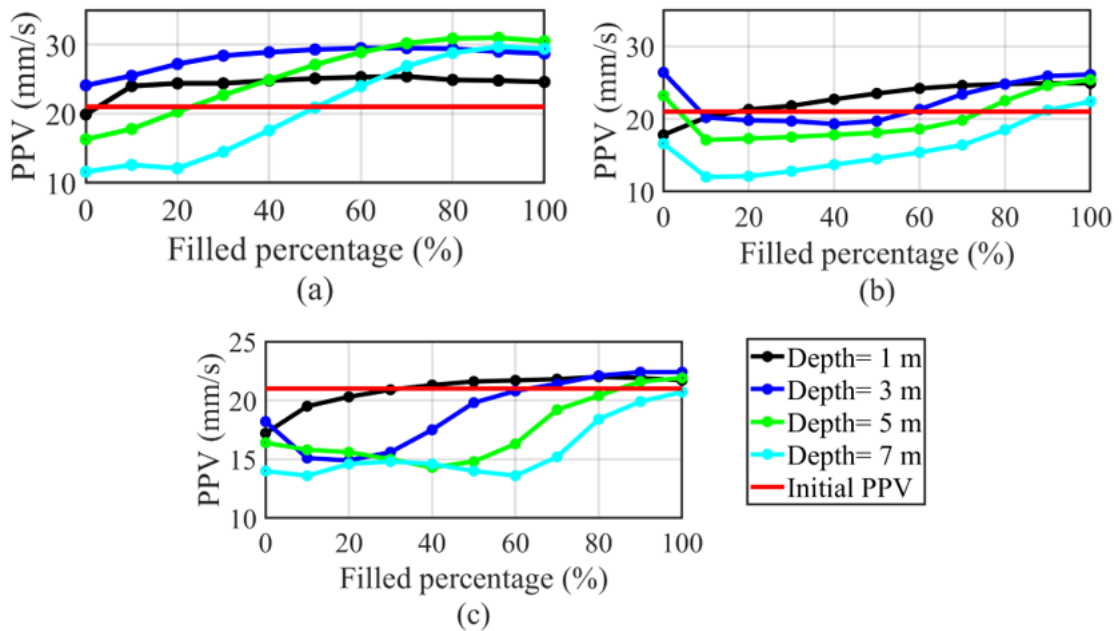

Fig. 12. Parametric study for partially concrete-filled single trenches located at a) 4 m, b) 8 m, c) 13 m.

Fig. 13 justifies the optimization results for dual trenches, a 7 m deep and a 2.9 m deep trench located at 4 m and 12.2 m, respectively. Parametric studies were not conducted for the quadruple trench configuration due to the massive computational cost. Nevertheless, the accuracy of the optimization procedure in the single and dual trench systems provides a strong assurance of correctness for the quadruple system.
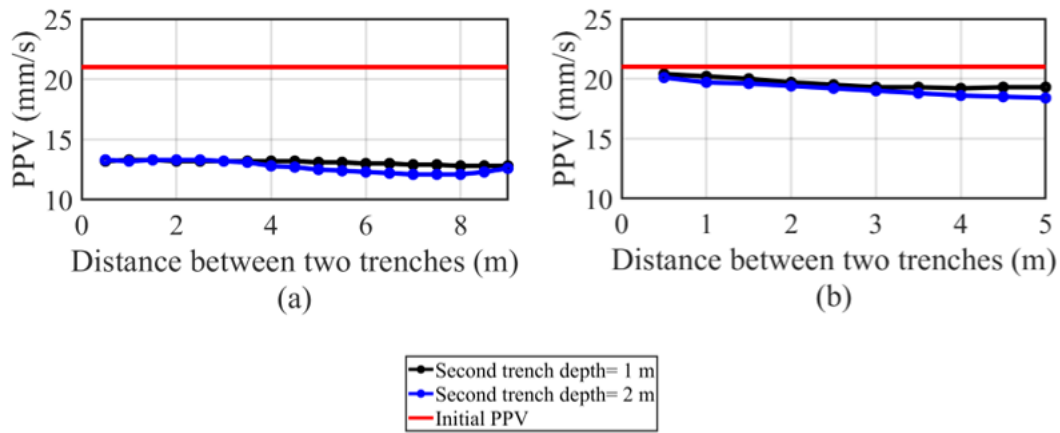

Fig. 13. Parametric study for dual-trenches. The first trench is located at a) 4 m, and b) 8 m from the centerline.

9. Practical implications of the study

From a practical perspective, vibration control is a common concern in many civil engineering projects. With the findings of this research, vibrations can be reduced in cases where DC-induced vibrations are important. While the use of barriers, which require significant cost and time, may not be necessary for simple projects, they are essential near critical structures like power plants and oil pipelines. In such cases, the importance of reducing vibrations as much as possible is paramount, as demonstrated by Wang et al. (2023) that considered the effects of direct current on oil pipelines, and utilized vibration isolation trenches to mitigate the resulting vibrations.

10. Conclusions

This research focuses on two main aspects; topology optimization of grout distribution within the design domain and the study of optimal rectangular trench configurations. This paper provides a comprehensive study of various trench types, including open, infilled, single, dual, and quadruple, specifically in the context of DC-induced vibrations.

In previous studies, many researchers have focused on investigating various factors affecting the performance of barriers. These problems need to be examined with a suitable tool due to the existing interdependencies between parameters, numerous affecting parameters, and the computational cost resulting from parametric studies. This research innovatively couples the finite element method and optimization to examine the performance of wave barriers in the context of dynamic compaction. Furthermore, while genetic algorithms have been used in some studies, this research employs a new and suitable algorithm called Covariance Matrix Adaptation Evolution Strategy. Additionally, the dispersion of materials in the soil for this type of loading has not been studied. Another innovation of this research is introducing the partially-filled barriers.

The significant findings of the current paper are as follows:

1. It is observed that open trenches exhibit the highest MC value. Moreover, the best open trench is a deep active one, a 7 m trench located 4 m from the tamping point, which yields an MC of 46%.

2. Generally, the most critical design parameter of the trenches is the depth, affecting the results significantly; however, not directly. Generally, it is detected that installing partially-filled trenches can be an innovative and useful method that results in a marginally higher MC.

3. Using dual and quadruple trenches instead of single trenches cannot lead to larger MC values. The increase is minor, and not practically recommended due to the need for more excavation and difficulties in practice.

4. In the case of distributing the grout within the domain, the final optimized layout takes a W-shaped configuration. The grout is mainly concentrated near the excitation source and in the proximity of the receiving point. The overall shape of the grout traps the waves in between, diminishing the vibration level in the domain. The concentration of grout near the excitation source minimizes the initial influence on the surrounding structures, and putting the grout in the proximity of the receiving point ensures blocking the propagated waves before they reach the critical point.

5. The numerical results are verified against field measurements, and the comparison reveals a perfect match.

6. The optimization results are verified by conducting a comprehensive parametric study, and a good match between verifications and optimization results guarantees the reliability of the proposed CMA-ES/FE optimization method. The findings of this study can be utilized to optimize trench design and construction techniques, mitigating vibrations, and improving overall performance.

7. Addressing certain limitations in the current research methodology and scope is essential. There are always simplifications and assumptions in numerical modelling that can affect the results. The main limitation of numerical modelling lies in the limited representation of real-world complexity. First, simplifying the system as an axisymmetric model may cause differences with real behaviour. Second, soil properties may vary in depth and length across the area of interest. Since the main consideration of this study is topology optimization, the model is simplified to a 2-D model and the variations of soil properties are not considered.

Disclosure statement

No potential conflict of interest was reported by the author(s).

References

Abaqus, F. (2014). Dassault systemes simulia corporation. *Providence, Rhode Island, USA*.

Abedini, F., Rafiee-Dehkharghani, R., & Laknejadi, K. (2022). Mitigation of vibrations caused by dynamic compaction considering soil nonlinearity. *International Journal of Civil Engineering*, *20*(7), 809-826. https://doi.org/10.1007/s40999-022-00700-9(0123456789().,-volV)(0123456789,-().volV)

Ahmad, S., & Al-Hussaini, T. (1991). Simplified design for vibration screening by open and in-filled trenches. *Journal of geotechnical engineering*, *117*(1), 67-88. https://doi.org/10.1061/(ASCE)0733-9410(1991)117:1(6

Alzawi, A. M. A. (2011). *Vibration isolation using in-filled geofoam trench barriers*. The University of Western Ontario (Canada).

Bayat, M., Saadat, M., & Hojati, A. (2023). Optimization of Dynamic Compaction Procedure for Sandy Soils. *Civil Engineering Infrastructures Journal*. https://doi.org/10.22059/CEIJ.2023.351287.1889

Bian, X., Cheng, C., Jiang, J., Chen, R., & Chen, Y. (2016). Numerical analysis of soil vibrations due to trains moving at critical speed. *Acta Geotechnica*, *11*, 281-294. https://doi.org/10.1007/s11440-014-0323-2

Cho, I. (2021). Wave energy dissipation by a floating horizontal porous plate in oblique incident waves. *Wave Motion*, *105*, 102765. https://doi.org/10.1016/j.wavemoti.2021.102765

Chopra, A. K. (2007). *Dynamics of structures*. Pearson Education India.

Croce, P., Flora, A., & Modoni, G. (2014). *Jet grouting: technology, design and control*. Crc Press.

Dolatshahi, K. M., Rezaie, A., & Rafiee-Dehkharghani, R. (2020). Topology optimization of wave barriers for mitigation of vertical component of seismic ground motions. *Journal of Earthquake Engineering*, *24*(1), 84-108. https://doi.org/10.1080/13632469.2017.1398694

Ekanayake, S. D., Liyanapathirana, D., & Leo, C. J. (2014). Attenuation of ground vibrations using in-filled wave barriers. *Soil Dynamics and Earthquake Engineering*, *67*, 290-300. https://doi.org/10.1016/j.soildyn.2014.10.004

Esmaeili, M., Zakeri, J. A., & Mosayebi, S. A. (2014). Investigating the optimized open V-shaped trench performance in reduction of train-induced ground vibrations. *International Journal of Geomechanics*, *14*(3), 04014004. https://doi.org/10.1061(ASCE)GM.1943-5622.0000331

Fathi Afshar, N., Hamidi, A., & Tavakoli Mehrjardi, G. (2024). Impact of diffraction on screening of dynamic compaction waves with barriers. *Innovative Infrastructure Solutions*, *9*(6), 184. https://doi.org/doi.org/10.1007/s41062-024-01502-9

Feng, S., Li, J., Zhang, X., Chen, Z., Zheng, Q., & Zhang, D. (2019). Numerical analysis of buried trench in screening surface vibration. *Soil Dynamics and Earthquake Engineering*, *126*, 105822. https://doi.org/10.1016/j.soildyn.2019.105822

Gao, M., & Shi, Z. (2019). A wave guided barrier to isolate antiplane elastic waves. *Journal of Sound and Vibration*, *443*, 155-166. https://doi.org/10.1016/j.jsv.2018.11.042

Groenwold, A. A., & Etman, L. (2010). A quadratic approximation for structural topology optimization. *International Journal for Numerical Methods in Engineering*, *82*(4), 505-524. https://doi.org/10.1002/nme.2774

Hansen, N. (2019). A global surrogate assisted CMA-ES. Proceedings of the genetic and evolutionary computation conference,

Hansen, N., & Auger, A. (2014). Evolution strategies and CMA-ES (covariance matrix adaptation). Proceedings of the Companion Publication of the 2014 Annual Conference on Genetic and Evolutionary Computation,

Hansen, N., Auger, A., Ros, R., Finck, S., & Pošík, P. (2010). Comparing results of 31 algorithms from the black-box optimization benchmarking BBOB-2009. Proceedings of the 12th annual conference companion on Genetic and evolutionary computation,

Herbut, A. (2020). Vibration mitigation efficiency of an inclined, curved, open trench. *PloS one*, *15*(2), e0229010. https://doi.org/10.1371/journal.pone.0229010

Jayawardana, P., Achuhan, R., De Silva, G. S., & Thambiratnam, D. (2018). Use of in-filled trenches to screen ground vibration due to impact pile driving: experimental and numerical study. *Heliyon*, *4*(8). https://doi.org/10.1016/j.heliyon.2018.e00726

Jayawardana, P., Thambiratnam, D. P., Perera, N., & Chan, T. (2019). Dual in-filled trenches for vibration mitigation and their predictions using artificial neural network. *Soil Dynamics and Earthquake Engineering*, *122*, 107-115. https://doi.org/10.1016/j.soildyn.2019.04.006

Jayawardana, P., Thambiratnam, D. P., Perera, N., Chan, T., & De Silva, G. S. (2019). Use of artificial neural network to evaluate the vibration mitigation performance of geofoam-filled trenches. *Soils and Foundations*, *59*(4), 874-887. https://doi.org/10.1016/j.sandf.2019.03.004

Jelušič, P., & Žlender, B. (2018). Optimal design of pad footing based on MINLP optimization. *Soils and Foundations*, *58*(2), 277-289. https://doi.org/10.1016/j.sandf.2018.02.002

Juang, C. H., & Wang, L. (2013). Reliability-based robust geotechnical design of spread foundations using multi-objective genetic algorithm. *Computers and Geotechnics*, *48*, 96-106. https://doi.org/10.1016/j.compgeo.2012.10.003

Kermani, A., Hamidi, A., & Asemi, F. (2024). MITIGATION OF TRANSIENT VIBRATIONS INDUCED BY DYNAMIC COMPACTION: A NUMERICAL STUDY ON THE EFFICACY OF OPEN TRENCH AND BOREHOLE BARRIERS.

Lukas, R. (1986). Dynamic compaction for highway construction, Design and construction guidelines, Volume I. *Federal Highway Administration Report FHWA-RD-86-133*.

Mahdavisefat, E., Heshmati, A., Salehzadeh, H., Bahmani, H., & Sabermahani, M. (2017). Vibration screening by trench barriers, a review. *Arabian Journal of Geosciences*, *10*, 1-14. https://doi.org/10.1007/s12517-017-3279-3

Majumder, M., & Venkatraman, S. (2023). A state-of-the-art review paper on the vibration screening techniques using open and in-filled trenches. *Asian Journal of Civil Engineering*, *24*(7), 2693-2708. https://doi.org/doi.org/10.1007/s42107-023-00613-5

Mayne, P. W., & Jones Jr, J. S. (1983). Impact stresses during dynamic compaction. *Journal of geotechnical engineering*, *109*(10), 1342-1346.

Mehdipour, S., & Hamidi, A. (2017). Impact of tamper shape on the efficiency and vibrations induced during dynamic compaction of dry sands by 3D Finite Element modeling. *Civil Engineering Infrastructures Journal*, *50*(1), 151-163. https://doi.org/10.7508/CEIJ.2017.01.009

Moussa, A., & El Naggar, H. (2020). Numerical evaluation of buried wave barriers performance. *International Journal of Geosynthetics and Ground Engineering*, *6*, 1-13. https://doi.org/10.1007/s40891-020-00240-z

Norén-Cosgriff, K., Bjørnarå, T. I., Dahl, B. M., & Kaynia, A. M. (2019). Advantages and limitation of using 2-D FE modelling for assessment of effect of mitigation measures for railway vibrations. *Applied Acoustics*, *155*, 463-476. https://doi.org/10.1016/j.apacoust.2019.06.013

Pan, J., & Selby, A. (2002). Simulation of dynamic compaction of loose granular soils. *Advances in Engineering Software*, *33*(7-10), 631-640. https://doi.org/10.1016/S0965-9978(02)00067-4

Persson, P. (2013). Reduction in ground vibrations by the use of wave obstacles.

Rafiee-Dehkharghani, R., Bansal, D., Aref, A. J., & Dargush, G. F. (2018). Analysis and optimal design of stress wave intensity attenuation in layered structures. *International Journal of Structural Stability and Dynamics*, *18*(01), 1850015. https://doi.org/10.1142/S0219455418500153

Rezaie, A., Rafiee-Dehkharghani, R., Dolatshahi, K. M., & Mirghaderi, S. R. (2018). Soil-buried wave barriers for vibration control of structures subjected to vertically incident shear waves. *Soil Dynamics and Earthquake Engineering*, *109*, 312-323. https://doi.org/10.1016/j.soildyn.2018.03.020

Sadeghi, S., Abedini, F., Rafiee-Dehkharghani, R., & Laknejadi, K. (2021). Covariance matrix adaptation evolution strategy for topology optimization of foundations under static and dynamic loadings. *Computers and Geotechnics*, *140*, 104461. https://doi.org/10.1016/j.compgeo.2021.104461

Saikia, A., & Das, U. K. (2014). Analysis and design of open trench barriers in screening steady-state surface vibrations. *Earthquake Engineering and Engineering Vibration*, *13*, 545-554. https://doi.org/10.1007/s11803-014-0261-x

Scott, R., & Pearce, R. (1975). Soil compaction by impact. *Geotechnique*, *25*(1), 19-30.

Seitz, K.-F., & Grabe, J. (2016). Three-dimensional topology optimization for geotechnical foundations in granular soil. *Computers and Geotechnics*, *80*, 41-48. https://doi.org/10.1016/j.compgeo.2016.06.012

Sigmund, O., Schevenels, M., Lazarov, B. S., & Lombaert, G. (2016). Topology optimization of two-dimensional elastic wave barriers. *Journal of Sound and Vibration*, *376*, 95-111. https://doi.org/10.1016/j.jsv.2016.04.039

Svinkin, M. R. (2004). Minimizing construction vibration effects. *Practice periodical on structural design and construction*, *9*(2), 108-115. https://doi.org/10.1061(ASCE)1084-0680(2004)9:2(108)

Tandon, K., Kumar, D., Ayothiraman, R., Manna, B., & Ramana, G. (2023). Numerical evaluation of tire chips–filled trench barriers for effective vibration isolation. *Journal of Low Frequency Noise, Vibration and Active Control*, *42*(1), 325-344. https://doi.org/doi.org/10.1177/146134842211189

Toraldo, C., Modoni, G., Ochmański, M., & Croce, P. (2018). The characteristic strength of jet-grouted material. *Geotechnique*, *68*(3), 262-279. https://doi.org/10.1680/jgeot.16.P.320

Wang, G., Yin, Y., & Wang, J. (2023). Vibration safety evaluation and vibration isolation control measures for buried oil pipelines under dynamic compaction: A case study. *Soil Dynamics and Earthquake Engineering*, *167*, 107783. https://doi.org/doi.org/10.1016/j.soildyn.2023.107783

Yarmohammadi, F., & Rafiee-Dehkharghani, R. (2020). An optimal design procedure of wave barriers for mitigation of underground and above-ground railway vibrations. *International Journal of Structural Stability and Dynamics*, *20*(11), 2050121. https://doi.org/10.1142/S0219455420501217

Yarmohammadi, F., Rafiee-Dehkharghani, R., Behnia, C., & Aref, A. (2018). Topology optimization of jet-grouted overlapping columns for mitigation of train-induced ground vibrations. *Construction and Building Materials*, *190*, 838-850. https://doi.org/10.1016/j.conbuildmat.2018.09.156

Zakeri, J.-A., Esmaeili, M., & Mosayebi, S.-A. (2014). Numerical investigation of the effectiveness of a step-shaped trench in reducing train-induced vibrations. *Proceedings of the Institution of Mechanical Engineers, Part F: Journal of Rail and Rapid Transit*, *228*(3), 298-306. https://doi.org/10.1177/0954409712473094